ChemComm

COMMUNICATION

View Article Online
View Journal | View Issue

Open Access Article. Published on 16 October 2020. Downloaded on 3/8/2026 4:35:47 AM.
This article is licensed under a Creative Commons Attribution-NonCommercial 3.0 Unported Licence.

Check for updates

Cite this: *Chem. Commun.*, 2020, **56**, 14251

Received 12th August 2020,
Accepted 16th October 2020

DOI: 10.1039/d0cc05483f

rsc.li/chemcomm

Unravelling the cellular emission fingerprint of the benchmark G-quadruplex-interactive compound Phen-DC$_3$†

Marco Deiana, Jan Jamroskovic, Ikenna Obi and Nasim Sabouri *

Phen-DC$_3$ is among the most commonly used G-quadruplex (G4)-stabilizers *in vitro* and in cells. Here, we show that the G4-interactive binding interactions enable one to tune the optical properties of Phen-DC$_3$ allowing the detection of G4 structures in cancer cells. This work opens up new directions for the use of Phen-DC$_3$ as a selective G4 fluorescent reporter.

G-Quadruplexes (G4s) are non-canonical four-stranded DNA and RNA structures formed by co-planar guanine-quartets stabilized through Hoogsteen-type hydrogen bonding and centrally octa-coordinated by monovalent cations.[1] Recent evidences suggest the involvement of G4 structures in key biological functions, such as replication, transcription, translation, and telomere maintenance.[2] Moreover, bioinformatics and sequencing studies have highlighted the widespread distribution of evolutionary conserved putative G4 sites in the genomes of humans and different model organisms.[2–5] Collectively, these findings have stimulated research probing G4-associated mechanisms and consequent opportunities for therapeutic intervention. This has led to the development of small-molecule therapeutics that can selectively bind, detect and stabilize these non-B DNA globular structures.[2] The majority of current G4 binders contain polyaromatic heterocyclic ring systems functionalized with flexible substituents.[2] This simple but efficient molecular design approach ensures both π–π stacking interactions between the terminal G-quartets and the central ligand's core and additionally electrostatic or ionic attractions between the pendant ligand's arms and the G-quadruplex's grooves. The phenanthroline dicarboxamide bisquinolinium compound, Phen-DC$_3$, is one of the most potent G4-binders reported so far and is used as a benchmark compound in a wide number of studies to probe G4 formation *in vitro* and in cellular systems.[6–16] Its overall crescent-like bent shape ensures an extensive overlap with the guanines on the terminal G-quartets and prevents intercalation between the Watson–Crick base pairs in duplex DNA, therefore limiting off-target binding interactions (Fig. 1).[2]

The weak fluorescence emission of Phen-DC$_3$ has been proven to be the major bottleneck of this compound to diagnostic transformation.[8] Indeed, *in situ* post-labeling by copper(I)-catalyzed 1,3-dipolar azide–alkyne cycloaddition (CuAAC) and strain-promoted azide–alkyne cycloaddition (SPAAC) click reactions were used to probe the cellular emission fingerprint of Phen-DC$_3$-based compounds in cancer cells.[8] These methods did not provide unambiguous evidences of Phen-DC$_3$'s cellular localization and showed inherent drawbacks including the need for *ad hoc* Phen-DC$_3$ structural optimization through laborious multi-step synthetic procedures as well as the possibility of artefactual staining by intermediate species when using ligands post-labeled by CuAAC. Therefore, there is still an urgent need to decipher the intracellular localization of Phen-DC$_3$ and answer open questions concerning its ability to track DNA and RNA G4 structures in cancer cells. Herein, we shed light on the ability of Phen-DC$_3$ to be used as an intrinsically fluorescent probe and we unravel its in-cell fate in the particular context of G4 recognition, opening new routes to advance future studies of G4 biology.

The absorption spectrum of Phen-DC$_3$ was monitored by UV-VIS spectroscopy and showed an intense well-structured band in

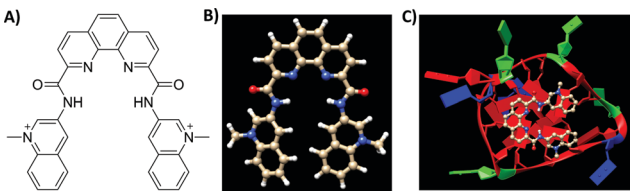

Fig. 1 (A and B) Chemical structure of Phen-DC$_3$ and related ball-and-stick model. (C) Solution structure of c-MYC Pu24T–Phen-DC$_3$ complex (PDB code: 2MGN).[6] Guanine, thymine and adenine bases are shown in red, green and blue, respectively.

Department of Medical Biochemistry and Biophysics, Umeå University, Umeå 90187, Sweden. E-mail: nasim.sabouri@umu.se

† Electronic supplementary information (ESI) available. See DOI: 10.1039/d0cc05483f

Open Access Article. Published on 16 October 2020. Downloaded on 3/8/2026 4:35:47 AM.
This article is licensed under a Creative Commons Attribution-NonCommercial 3.0 Unported Licence.

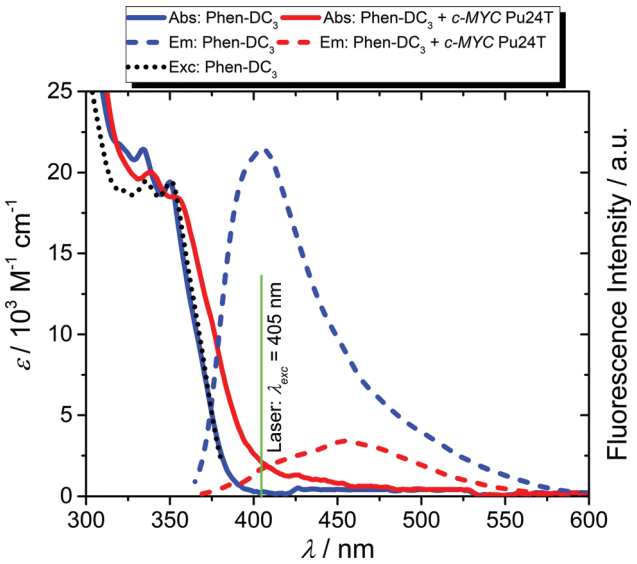

Fig. 2 Absorption (solid lines) and fluorescence (dashed lines) spectra of Phen-DC_3 in the absence (blue lines) and presence (red lines) of an equimolar concentration of c-MYC Pu24T (c_{tris} = 50 mM, c_{KCl} = 100 mM, $c_{Phen\text{-}DC_3}$ = 2.5 or 5.0 μM and $c_{c\text{-}MYC\,Pu24T}$ = 0.0, 2.5 or 5.0 μM for emission and absorption, respectively, λ_{exc} = 350 nm). The excitation spectrum of Phen-DC_3 is represented by the black dotted line. The green solid line indicates the diode laser's excitation wavelength at 405 nm used for CLSM.

the UV-spectral region with the maximum (λ_{max}) centered at 350 nm and extinction coefficient $\varepsilon \sim 2.0 \times 10^4$ M^{-1} cm^{-1} (Fig. 2). The addition of an equimolar concentration of c-MYC Pu24T, a widely used model parallel G4 structure derived from the oncogenic c-MYC promoter[6] (Fig. S1, ESI†), to Phen-DC_3 resulted in the concomitant bathochromic shift of its absorption maximum (~355 nm) and the appearance of a long-wavelength tail that extended over the blue region of the spectrum (Fig. 2).

Similar spectral changes were observed for Phen-DC_3 complexed with a hybrid telomeric G4-forming sequence, Tel-22, and a parallel RNA G4 structure, $4G_3U_3$ (Fig. S1–S3, ESI†).[9] This evolution pattern suggests that Phen-DC_3 may be sensitive to viscosity and/or polarity changes. To test this hypothesis, we recorded the UV-VIS absorption spectra of Phen-DC_3 in pure water as well as in a highly viscous H_2O : glycerol (50 : 50) binary mixture (Fig. S4, ESI†). No relevant spectral changes were observed in the absorption band of Phen-DC_3 ruling out spectral modifications associated with viscosity changes. On the other hand, Phen-DC_3, in methanol (MeOH), showed similar spectral changes to those observed with DNA or RNA G4 structures (Fig. S5, ESI†). In particular, the appearance of a long-wavelength tail suggests that Phen-DC_3 is sensitive to the matrix polarity and its accommodation within the hydrophobic G4 scaffold well matched a relative polarity value (E_T^N) of 0.76.[17] We also recorded the fluorescence spectrum of Phen-DC_3, and upon photoexcitation at 350 nm, an emission maximum (λ_{em}) at ~405 nm was observed (Fig. 2). The addition of an equimolar concentration of c-MYC Pu24T significantly quenched and red-shifted the emission band of Phen-DC_3 (Fig. 2). Similar optical changes were observed for Phen-DC_3 complexed with Tel-22 or $4G_3U_3$ (Fig. S6, ESI†). Due to the resulting low molecular brightness of the Phen-DC_3–G4 complexes, excitation at 405 nm did not provide enough sensitivity to detect the associated luminescence band of Phen-DC_3's bound states by using conventional steady-state emission spectroscopy. Nevertheless, this outcome did not preclude its implementation as a cellular G4-selective fluorescent reporter in confocal laser scanning microscopy (CLSM, *vide infra*).

In order to further examine the interaction of c-MYC Pu24T DNA and Phen-DC_3, we determined Phen-DC_3's stabilization properties of c-MYC Pu24T and a non-G4 DNA control. We performed the Taq-polymerase stop assay, a type of primer extension assay that determines DNA replication progression and pausing at single nucleotide resolution.[18] We found that increasing the concentration of Phen-DC_3 induced an increased G4 stabilization response, which resulted in the inhibition of DNA replication and a clear pausing site one nucleotide before the first G-tract (Fig. 3A). The pausing site on the c-MYC Pu24T template was already detected at 8 nM, while the synthesis of the non-G4 template was unaffected at this concentration. High concentrations of Phen-DC_3 (2 and 5 μM) caused non-specific inhibition of DNA replication on both the G4 and non-G4 DNA templates showing a wide window of selectivity between G4 and non-G4 DNA structures (Fig. 3A and B). To further investigate the ability of Phen-DC_3 to induce G4 stabilization on the c-MYC

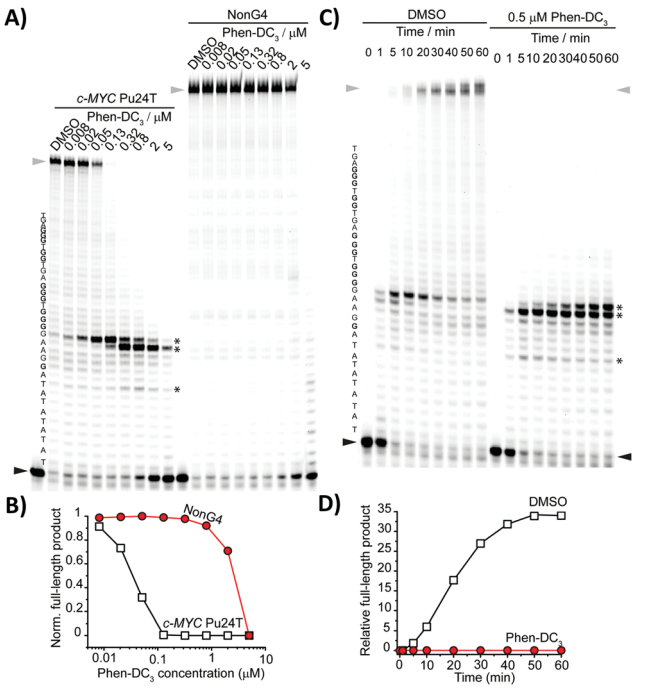

Fig. 3 (A) Dose-dependent Taq-DNA polymerase stop assay with different Phen-DC_3 concentrations using c-MYC Pu24T and non-G4 DNA templates. (B) Gel quantification of full-length product normalized to the DMSO control sample of the gel in (A). (C) Time-dependent Taq-DNA polymerase stop assay using Phen-DC_3 (0 and 0.5 μM) and c-MYC Pu24T as the G4 template. (D) Gel quantification of full-length products of the gel in (C). The G4 sequence is presented on the left side of the gels in (A and C). Guanines involved in the formation of the G4 motif are in bold. Asterisks indicate pausing sites; the black arrow indicates the start of the reaction and the grey arrow full-length products.

Open Access Article. Published on 16 October 2020. Downloaded on 3/8/2026 4:35:47 AM.
This article is licensed under a Creative Commons Attribution-NonCommercial 3.0 Unported Licence.

Pu24T template, we monitored the replication progression by primer extension assay over time (Fig. 3C and D). G4-Mediated formation of pausing sites was visible after 1 minute in both untreated and Phen-DC_3-treated samples. With time progression, the pausing site in the control sample slowly disappeared, showing that allowing multiple attempts by the DNA polymerase to bypass the G4 structure induces G4 destabilization and eventually results in bypass of the G4 structures by the DNA polymerase. However, in Phen-DC_3-treated samples, the pausing site was detected even after 60 mins of incubation and the synthesis of the full-length product was completely inhibited (Fig. 3C and D), indicating that Phen-DC_3 is indeed a highly potent G4 stabilizer.

The G4-interactive binding properties of Phen-DC_3 along with its optical changes characterized by a long-wavelength absorption tail and a red-shifted emission maximum, prompted us to study the cellular localization of Phen-DC_3 in human cervical carcinoma (HeLa) cells by CLSM. Indeed, the spectral changes of Phen-DC_3 in the presence of DNA and RNA G4s that led to a considerable increase in absorption at 405 nm, matches well to the excitation laser line setting used in CLSM (Fig. 2 and Fig. S2, S3, ESI†). This "double-check" detection mechanism based on binary conditions (OFF–ON absorption states at 405 nm) exclusively enables the cellular visualization of the active fluorescent bound states (Phen-DC_3–G4 complexes) limiting issues related to off-target effects and low signal-to-noise ratio. A limit of detection (LOD) of 582 ± 9 nM was calculated by monitoring the changes in the optical density at 405 nm as a function of G4 concentration (Fig. S7, ESI†). This LOD value, even if slightly higher compared to the most sensitive light-up G4 probes reported so far, still falls within the nanomolar range and provides possibilities to probe G4 formation in a cellular context.[16,19,20] The treatment of PFA-fixed HeLa cells with Phen-DC_3 showed an intense fluorescence signal in the cytoplasmic and nuclear regions with clear peaks in the subnuclear compartments whose appearance is compatible with nucleoli (Fig. 4A and B).[16,19,21,22] The observed staining pattern was independent of the fixation method, as Phen-DC_3-treated cells fixed with MeOH showed a similar staining pattern but with reduced cytoplasmic signal (Fig. S8, ESI†).

Under the same experimental conditions used to image the Phen-DC_3-stained cells, untreated cells did not show any fluorescence signal (Fig. 4A), showing that the fluorescence observed in Phen-DC_3-treated cells is not due to auto-fluorescence of cells. Together, these data show that Phen-DC_3 can be visualized in fixed cells (Fig. 4A, B and Fig. S8, ESI†).

The G4-specific BG4 antibody showed the occurrence of G4 structures at both cytoplasmic and nuclear regions indicating cellular formation of RNA and DNA G4s, respectively.[23,24] Phen-DC_3 targets both RNA and DNA G4 structures with nanomolar dissociation constants.[9,25] Therefore, the staining pattern of Phen-DC_3 may be directly related to its ability to target RNA G4s in the cytoplasm and DNA G4s in the nucleus. To elucidate the nature of the main cellular binding targets of Phen-DC_3, we pretreated the cells with either RNase or DNase before incubation with Phen-DC_3. RNase pretreatment did not affect

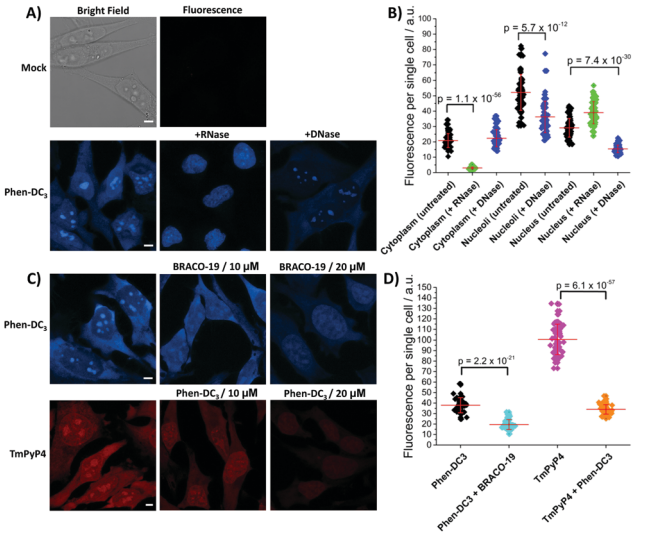

Fig. 4 Microscopy imaging of PFA-fixed HeLa cells. (A) Bright field image and/or confocal fluorescence images of unstained or Phen-DC_3-stained (20 μM) cells. Where denoted, the fixed cells were pre-treated with either RNase or DNase prior to Phen-DC_3-treatment. (B) Quantification of the fluorescence signal per single cell. Data represent quantification of 60 individual cells for each condition. Signals from nucleoli in RNase-treated cells could not be quantified. Means ± SD are indicated. Data were analyzed using two-sample *t* tests. *P*-values are indicated. (C) Fluorescence displacement assay (upper panel) between Phen-DC_3 (20 μM) and BRACO-19 (10 and 20 μM). Fluorescence displacement assay (lower panel) between TmPyP4 (10 μM) and Phen-DC_3 (10 and 20 μM). (D) Quantification and analysis as in (B). Phen-DC_3–BRACO-19 competition (n = 40 for each condition) and TmPyP4–Phen-DC_3 competition (n = 55 for each condition). Scale bar = 5 μm. A diode 405 nm laser was used for Phen-DC_3 λ_{exc} = 405 nm, λ_{em} 430–630 nm; an argon laser was used for TmPyP4 visualization λ_{exc} = 514 nm, λ_{em} = 550–700 nm.

the nuclear staining pattern of Phen-DC_3 but reduced its cytoplasmic ($p = 1.1 \times 10^{-56}$) and nucleolar signal, supporting binding of Phen-DC_3 to RNA molecules in these two cellular regions (Fig. 4A, B and Fig. S8, ESI†). RNase treatment caused almost complete disappearance of the Phen-DC_3-associated fluorescence signal in the nucleoli. Conversely, DNase treatment significantly reduced the nuclear staining ($p = 7.4 \times 10^{-30}$) and to some extent the nucleolar signal ($p = 5.7 \times 10^{-12}$) by Phen-DC_3, but its cytoplasmic signal was almost unperturbed (Fig. 4A, B and Fig. S8, ESI†). Together, these RNase/DNase-treated cell data suggest that Phen-DC_3 mainly targets RNA G4s in both cytoplasmic and nucleolar regions and DNA G4s in the nucleus. In order to confirm that only the bound Phen-DC_3–DNA/RNA G4s states were responsible for the fluorescence emission observed in cells, we pre-treated the cells simultaneously with both DNase and RNase (Fig. S8, ESI†). No fluorescence signal was observed for Phen-DC_3 under these experimental conditions, suggesting that the detected fluorescence observed in cells is due to Phen-DC_3 being in complex with DNA and RNA G4s.

In order to further probe the sensing ability of Phen-DC_3 when targeting G4 structures in cells, we performed two independent fluorescence displacement assays using the well-known G4-binders BRACO-19[2] and TmPyP4[2] (Fig. 4C and D). Direct competition performed by adding BRACO-19 to

Open Access Article. Published on 16 October 2020. Downloaded on 3/8/2026 4:35:47 AM.
This article is licensed under a Creative Commons Attribution-NonCommercial 3.0 Unported Licence.

Phen-DC_3-pretreated cells showed a clear reduction of the cytoplasmic and nucleolar Phen-DC_3 fluorescence signal ($p = 2.2 \times 10^{-21}$), indicating the effective competition between these two molecules for the same G4-sites, mostly at the RNA level (Fig. 4C and D). TmPyP4 is a porphyrin-based fluorescent duplex/G4 binder, and its absorption and emission spectra are more red-shifted than Phen-DC_3. Cells treated with TmPyP4 demonstrated a similar staining pattern as Phen-DC_3. Indeed, the addition of Phen-DC_3 to cells pretreated with TmPyP4, resulted in an overall fluorescence signal reduction ($p = 6.1 \times 10^{-57}$) at both the extranuclear and nuclear level, demonstrating the high degree of co-localization between these two G4-binders (Fig. 4C and D). The remaining weak nuclear fluorescence signal that still occurred upon Phen-DC_3-mediated TmPyP4 displacement may be ascribed to the well-known ability of the porphyrin ligand to intercalate duplex DNA, making these DNA sites highly inaccessible to Phen-DC_3.[2]

Non-cancerous human embryonic kidney (HEK 293) cells were also used to ascertain that the Phen-DC_3 emission recorded was not strictly correlated to the cell-type used (Fig. S9, ESI†). Under the same experimental conditions used to image HeLa cells, HEK 293 cells treated with Phen-DC_3 showed a very similar staining pattern with most of the associated signal confined within the nucleolar sites. Direct quantitative comparison of the G4 levels present in these two cell lines was not performed because the two cell types are not derived from the same tissue, and therefore the G4 levels cannot be compared.

In conclusion, we have reported for the first time, the cellular localization of one of the most potent and widely used G4 ligands, Phen-DC_3. We demonstrate that Phen-DC_3 can be used to image cells without the need of any chemical modification. A set of cellular-based fluorescence experiments clearly showed the sensing ability of Phen-DC_3 when targeting RNA G4s in both the cytoplasm and nucleoli, and DNA G4s in the nucleus. This report opens up new directions and possibilities for the use of Phen-DC_3 to track non-canonical DNA structure formations in different cellular contexts.

This work was supported by the Knut and Alice Wallenberg Foundation (KAW2015-0189), the Swedish Research Council (VR-MH 2018-02651), and the Swedish Cancer Society (CAN19 0126). MD was supported by a fellowship from the MIMS Excellence by Choice Postdoctoral Program. We thank Dr Tamilselvi Shanmugam and Dr Irene Martinez Carrasco for their expert advice regarding microscopy. The authors thank the Biochemical Imaging Center at Umeå University and the National Microscopy Infrastructure (VR-RFI 2016-00968). We thank Dr Paulina Wanrooij for the kind gift of the HEK 293 cells.

Conflicts of interest

There are no conflicts to declare.

Notes and references

1 M. L. Bochman, K. Paeschke and V. A. Zakian, *Nat. Rev. Genet.*, 2012, **13**, 770–780.
2 S. Neidle, *J. Med. Chem.*, 2016, **59**, 5987–6011.
3 V. S. Chambers, G. Marsico, J. M. Boutell, M. Di Antonio, G. P. Smith and S. Balasubramanian, *Nat. Biotechnol.*, 2015, **33**, 877–881.
4 G. Marsico, V. S. Chambers, A. B. Sahakyan, P. McCauley, J. M. Boutell, M. Di Antonio and S. Balasubramanian, *Nucleic Acids Res.*, 2019, **47**, 3862–3874.
5 N. Sabouri, J. A. Capra and V. A. Zakian, *BMC Biol.*, 2014, **12**, 101.
6 W. J. Chung, B. Heddi, F. Hamon, M.-P. Teulade-Fichou and A. T. Phan, *Angew. Chem., Int. Ed.*, 2014, **53**, 999–1002.
7 A. De Cian, E. DeLemos, J.-L. Mergny, M.-P. Teulade-Fichou and D. Monchaud, *J. Am. Chem. Soc.*, 2007, **129**, 1856–1857.
8 J. Lefebvre, C. Guetta, F. Poyer, F. Mahuteau-Betzer and M.-P. Teulade-Fichou, *Angew. Chem., Int. Ed.*, 2017, **56**, 11365–11369.
9 K. Halder, E. Largy, M. Benzler, M.-P. Teulade-Fichou and J. S. Hartig, *ChemBioChem*, 2011, **12**, 1663–1668.
10 A. Piazza, J.-B. Boulé, J. Lopes, K. Mingo, E. Largy, M.-P. Teulade-Fichou and A. Nicolas, *Nucleic Acids Res.*, 2010, **38**, 4337–4348.
11 L. T. Gray, E. Puig Lombardi, D. Verga, A. Nicolas, M.-P. Teulade-Fichou, A. Londoño Vallejo and N. Maizels, *Cell Chem. Biol.*, 2019, **26**, 1681–1691.e5.
12 K. G. Zyner, D. S. Mulhearn, S. Adhikari, S. Martínez Cuesta, M. Di Antonio, N. Erard, G. J. Hannon, D. Tannahill and S. Balasubramanian, *eLife*, 2019, **8**, e46793.
13 I. Obi, M. Rentoft, V. Singh, J. Jamroskovic, K. Chand, E. Chorell, F. Westerlund and N. Sabouri, *Nucleic Acids Res.*, 2020, gkaa820, DOI: 10.1093/nar/gkaa820.
14 M. Wallgren, J. B. Mohammad, K.-P. Yan, P. Pourbozorgi-Langroudi, M. Ebrahimi and N. Sabouri, *Nucleic Acids Res.*, 2016, **44**, 6213–6231.
15 P. Prorok, M. Artufel, A. Aze, P. Coulombe, I. Peiffer, L. Lacroix, A. Guédin, J.-L. Mergny, J. Damaschke, A. Schepers, C. Cayrou, M. -P. Teulade-Fichou, B. Ballester and M. Méchali, *Nat. Commun.*, 2019, **10**, 3274.
16 M. Deiana, K. Chand, J. Jamroskovic, I. Obi, E. Chorell and N. Sabouri, *Angew. Chem., Int. Ed.*, 2020, **59**, 896–902.
17 C. Reichardt, *Chem. Rev.*, 1994, **94**, 2319–2358.
18 J. Jamroskovic, M. Livendahl, J. Eriksson, E. Chorell and N. Sabouri, *Chem. – Eur. J.*, 2016, **22**, 18932–18943.
19 M. Deiana, K. Chand, J. Jamroskovic, R. N. Das, I. Obi, E. Chorell and N. Sabouri, *Nanoscale*, 2020, **12**, 12950–12957.
20 M. Zuffo, A. Guédin, E.-D. Leriche, F. Doria, V. Pirota, V. Gabelica, J.-L. Mergny and M. Freccero, *Nucleic Acids Res.*, 2018, **46**, e115.
21 J. Jamroskovic, M. Doimo, K. Chand, I. Obi, R. Kumar, K. Brännström, M. Hedenström, R. N. Das, A. Akhunzianov, M. Deiana, K. Kasho, S. Sulis Sato, P. L. Pourbozorgi, J. E. Mason, P. Medini, D. Öhlund, S. Wanrooij, E. Chorell and N. Sabouri, *J. Am. Chem. Soc.*, 2020, **142**, 2876–2888.
22 J. Li, X. Yin, B. Li, X. Li, Y. Pan, J. Li and Y. Guo, *Anal. Chem.*, 2019, **91**, 5354–5361.
23 G. Biffi, D. Tannahill, J. McCafferty and S. Balasubramanian, *Nat. Chem.*, 2013, **5**, 182–186.
24 G. Biffi, M. Di Antonio, D. Tannahill and S. Balasubramanian, *Nat. Chem.*, 2014, **6**, 75–80.
25 L. Bonnat, L. Bar, B. Gennaro, H. Bonnet, O. Jarjayes, F. Thomas, J. Dejeu, E. Defrancq and T. Lavergne, *Chem. – Eur. J.*, 2017, **23**, 5602–5613.

 This journal is © The Royal Society of Chemistry 2020